DEPARTMENT OF PHYSICS,

SCHOOL OF SCIENCE AND ENGINEERING,

UNIVERSITY OF CRETE

"Optimization and characterization of photo-acoustic microscopy in reflection mode geometry"

Andreadaki Eleni

Ph4952

Scientific Supervisor : Dr. Ioannis Zacharakis

The thesis took place at Laboratory for Biophotonics and Molecular Imaging (LBMI) under the suvervision of group leader Dr. Ioannis Zaxarakis at IESL-FORTH

Table of contents

1.0 Abstract

Biomedical scientists have developed a variety of optical systems in different geometries and with a variety of characteristics that basically use the photoacoustic effect for imaging. This work was focused on the creation of such a system in reflection mode geometry. The main aim was the optimization and characterization of the set up after its construction. In more detail, firstly it was decided which kind of photoacoustic microscopy would be used, OR-PAM or AR-PAM. Later after making the choice of using the OR-PAM it was studied how the acoustic (transducer) and optical (objective) components would be combined in order to be able to produce a high acoustic signal. Furthermore after the selection of the appropriate combination, the next step was the improvement of the signal by choosing a suitable acoustic lens in front of the detector which would guide the ultrasound on the transducer. In addition it was taken under consideration which geometries of ultrasound transmission were more efficient, the use of a beam splitter or an ultrasound reflecting glass. Also after acquisition of the clear signal the characteristics of the modality, such as the typical value of the photoacoustic signal (V_{pp}), the signal to noise ratio, the frequency range of the transducer and lastly the field of view were determined. Finally the first images of the system with the help of phantoms were taken.

2.0 Περίληψη

Οι επιστήμονες της βιοϊατρικής έχουν αναπτύξει μια ποικιλία οπτικών συστημάτων σε διαφορετικές γεωμετρίες και χαρακτηριστικά που βασικά χρησιμοποιούν το φωτοακουστικό φαινόμενο για απεικόνιση. Έτσι λοιπόν αυτή η εργασία επικεντρώθηκε στη δημιουργία ενός τέτοιου συστήματος σε γεωμετρία ανάκλασης. Βασικός στόχος ήταν η βελτιστοποίηση και ο χαρακτηρισμός του συστήματος μετά την κατασκευή του. Αναλυτικότερα, αρχικά αποφασίστηκε ποιο είδος φωτοακουστικής μικροσκοπίας θα χρησιμοποιηθεί, OR-PAM ή AR-PAM. Αργότερα, αφού έγινε η επιλογή χρήσης του OR-PAM, μελετήθηκε ο τρόπος με τον οποίο θα συνδυάζονταν τα ακουστικά (ανιχνευτής υπερήχων) και τα οπτικά (αντικειμενικός φακός) στοιχεία προκειμένου να είναι σε θέση να παραχθεί ένα υψηλό ακουστικό σήμα. Επιπλέον, μετά την επιλογή του κατάλληλου συνδυασμού, επιδιώχθηκε να βελτιωθεί αυτό το σήματος επιλέγοντας κατάλληλο διορθωτικό φακό μπροστά από τον ανιχνευτή , ο οποίος θα καθοδηγούσε τον υπέρηχο σε αυτόν. Επιπλέον, ελήφθη υπόψη ποιοι τρόποι μετάδοσης υπερήχων ήταν πιο αποτελεσματικοί, ένας κυβικός διαχωριστής δέσμης ή ένα γυαλί ανάκλασης υπερήχων. Τέλος μετά την απόκτηση του καθαρού σήματος προσδιορίστηκαν τα χαρακτηριστικά του συστήματος, όπως η τυπική τιμή του φωτοακουστικού σήματος (Vpp) που έδινε, ο λόγος σήματος προς θόρυβο, το εύρος συχνοτήτων του ανιχνευτή που εντοπιζόταν και τέλος το οπτικό πεδίο που έδινε. Τελικά λήφθηκαν οι πρώτες εικόνες του συστήματος με τη βοήθεια δειγμάτων προσομοίωσης.

3.0 Introduction

Simple microscopes with only one lens were the first imaging modality that were developed to depict the morphology of a variety of objects. Later with the improvement of microscopes with two lenses (objective and preophthalmic) information about the morphology of the cell walls and nuclei were known. In fact, in this period of time the cells theory was established. Later with the invention of lasers and the deeper understanding about the basic principles of sciences such physics, the imaging modalities further improved. Especially microscopes became more complex systems because they were combining light from lasers and from a bulb and depending on the application, they presented different characteristics. Their functionallity was based on the interaction between light and matter and new techniques were developed such as fluorescence microscopy. As the time gone by a new method surfaced which used the photoacoustic effect to transform photon energy into ultrasonic energy and consequently a new path in biomedical imaging was created.

In particullar, photoacoustic imaging has become a rapidly developing new biomedical imaging modality. A great advantage is the fact that it has surpassed the optical diffusion limit that other pure optical imaging techniques have. As result more information about a researched biological sample could be gathered. Photoacoustic imaging has been used to measure brain metabolism, micro vessels and lymph nodes, melanoma detection, breast cancer and oxygenation. To make all these measurements possible, biomedical scientists constructed, with the help of physicist and programmers, suitable system such as photoacoustic tomographers (PAT) and photoacoustic microscopes (PAM). Today PAM is widely used in biomedical for the imaging of the anatomical, functional, molecular, flow dynamic, and metabolic differences in tissues.

4.0 Theory

Fundamental life science and clinical practice have undergone revolutionary changes for centuries thanks to the creation of optical microscopes. And so optical microscopy had become the most popular imaging modality in the biomedical world due to its superior image contrast in soft tissue. Also sharp optical focusing was necessary for optical microscopy to have its visual potency. Unfortunately a problem occurred. As photons penetrate further into biological tissue, a highly scattering medium for electromagnetic waves in the optical spectrum range, their power rapidly decreases. Photons often encounter tens of scattering events before they reach the optical diffusion limit (1 mm in tissue), which prevents tight focusing by randomizing the photon trajectories. Physicists have made little headway against scattering for decades by employing pure optical methods. Fortunately, the newly developed method of photoacoustic tomography (PAT), which uses the photoacoustic effect to transform photon energy into ultrasonic energy, has shown a new path.**[1]** The development of PAT was based on the interaction between matter and light and its results. Specifically engineers took into consideration the heat that is produced by an excited electron when the last one relax to the ground state. A major implementation of PAT is the photoacoustic microscopy (PAM) on which this thesis is based on.

4.1 Microscopy

To begin with it is important to define the concept of microscopy and its basic characteristics. Microscopy is the technical field of using microscopes to view objects and areas of objects that cannot be seen with the human eye because these objects are not within the resolution range of the eye.**[2]** Specifically in biological microscopy there are two types of illumination transillumination or epillumination. In transillumination, light from the source is collected and shaped by the condenser, travels through the sample, and is magnified by the objective and then by eyepieces. **[3]** In epi-illumination, light travels through the objective, which also acts as a condenser. Light reflected or emitted by the sample enters the objective and is separated from excitation light by dichroic mirrors.**[3][4]**

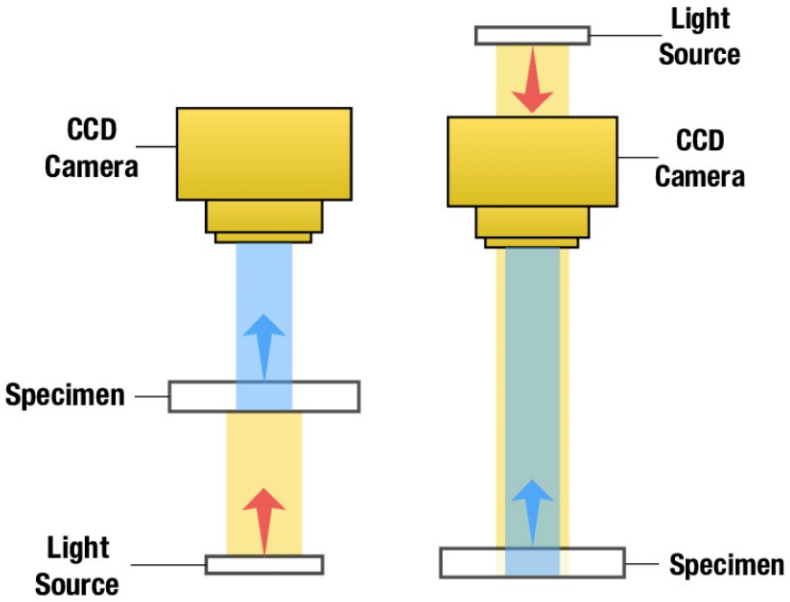

Figure 4.1: Types of illumination : (a) Trans-illumination (b) epi-illumination ***[5]***

In addition when a scientist tries to plan an imaging experiment by using an optical microscope he should take in consideration the lateral resolution, the depth of field (DOF), the field of view, the numerical aperture (NA) of the objective/condenser combination and its magnitude and finally the light wavelength, for the experiment to work better. The above therms will be analyzed later.

4.1.1 Light source

Depending on the application that an optical microscope will be used, it may have different light sources such as a light bulb or a laser source. The light that is emitted by light bulb is not coherent. It shines in different directions and shows different wavelengths. Typically the entire spectrum of the visible light is covered. A laser beam is coherent light**[6]**, which exhibits certain attributes. Firstly it is electromagnetic radiation that has a certain wavelength and it is usually a single-colour light, which means single wavelength. This wavelength determines the beam's colour. In addition, the waves are "synchronized", they shine in the same direction, they swing in the same level and in the same phase. All descriptive

parameters (frequency, polarization and phase) are in a fixed spatial and temporal context and as a result they reinforce electromagnetic waves by overlapping. In bio imaging the microscopes use laser beams for the imaging of the tissue and molecules and light bulbs to optical focus the objective lens.

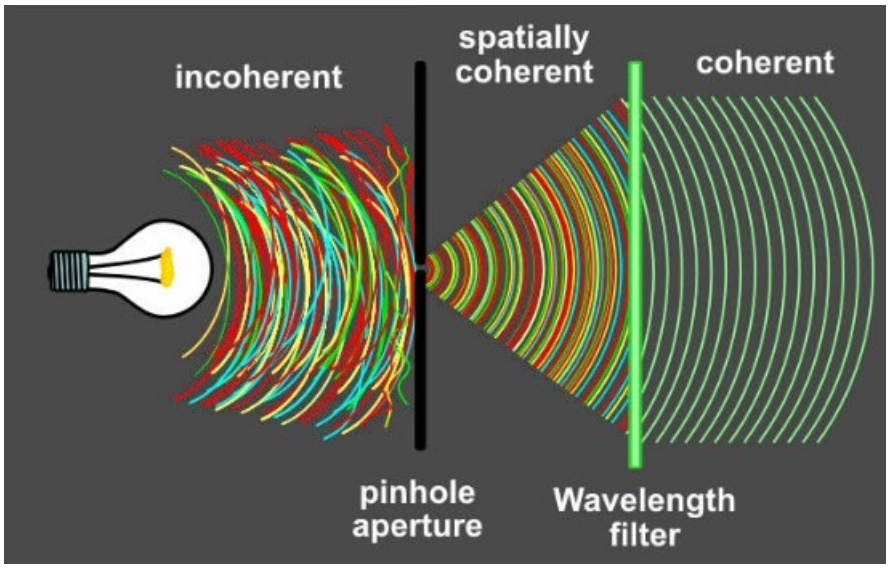

Figure 4.2: Demostration of Incoherent and Coherent light [7]

4.1.2 Numerical Aperture

NA depends on the objective construction, working distance, and the refraction coefficient n of the immersion medium: $NA = n\sin(a)$ (eq. 4.1) where α is the maximum light cone angle. When the NA is large it is correct to imply that the magnification of the objective is higher and therefore the lateral resolution is higher. **[3]**

4.1.3 Resolution

In general for the lateral resolution it applies that the shorter the wavelength of transmitted light and the larger the NA, the finer the details, that can be distinguished in the XY plane (higher resolution), are. In transillumination, the theoretical distance r between minimally distinguishable points is: $r = \frac{1{,}22\,\lambda}{NA_{cons} + NA_{obj}}$

(eq. 4.2) and in epi-illumination: $r=\frac{0,61\lambda}{NA_{obj}}$ (eq. 4.3). Also since short-wavelength light, which provides the best resolution for, is more readily absorbed by tissue and scattered, there is a trade-off between resolution and depth of tissue penetration. **[3]**

On the other hand the axial resolution expresses how small objects someone could observe along the propagation axis. In some cases, like fluorescence, it is considered the same as the depth of field but in others, like photoacoustics, are different properties.

4.1.4 Depth of field

The distance between the nearest and farthest object planes that are still in focus is known as the depth of field (DOF). DOF could be calculated with the help the equation : $DOF=\frac{n\lambda}{NA^2}$ (eq. 4.4)

In addition from the equation 4.4 can be seen that larger magnification objectives have smaller DOF. This small DOF can provide fine optical sectioning of the sample. As shown in equation above both wave and geometrical optics components can define DOF. In fact the wave component is inversely proportional to the square of the NA. The larger the NA the higher the 3D resolution. To conclude the DOF for coherent light (e.g., laser) could differ from that predicted by the equation.**[3]**

4.1.5 Magnification

Magnification and Resolution are often confused as the same but they are not. Magnification is the process of enlarging the apparent size not physical size, of an object or a tissue or an image. This enlargement is quantified by a calculated number

M also called "magnification". The magnification of lenses (linear) is given by the equation $M=\frac{f}{f-d_0}$ (eq. 4.5) where f is the focal length and d_0 is the distance from the lenses to object. For magnifying glass the maximum angular magnification

(compared to the naked eye) of a magnifying glass depends on how the glass and the object are held, relative to the eye.

If the lens is held at a distance from the object such that its front focal point is on the object being viewed, the relaxed eye (focused to infinity) can view the image with angular magnification $M_A = \frac{25\,cm}{f}$ (eq. 4.6), where f is the focal length of the lens in centimeters. The constant 25 cm is an estimate of the "near point" distance of the eye—the closest distance at which the healthy naked eye can focus. In this case the angular magnification is independent from the distance kept between the eye and the magnifying glass. Lastly for microscopes (angular) is given by $M_A = M_0 \times M_e$ (eq. 4.7) where M_e the magnification of the eyepiece, which depends upon its focal length f_e and M_0 the magnificatinon of the objective, which depends on its focal length f_0 and the distance d between objective back focal plane and the plane of the eyepiece(tube length). **[6]**

4.1.6 Field of view

Field of view (also abbreviated as FOV) for a microscope is the extent of the observable area in distance units. The optics provide a clear and undistorted view in a field around the optical axis, and the field of view is selected from this. The rays that produce the image in this view are generally aberration-free and do not create a significant falloff in image intensity. Furthermore as the magnification increases, the field of view is reduced **[8]**.

4.2 Photoacoustic effect

After the little introduction about microscopy it is time to present the photoacoustic effect. The photoacoustic effect is a phenomenon in which ultrasounds waves are generated by the thermoelastic expansion of materials or tissues excited with nonionizing electromagnetic waves, such as, short-pulsed laser light. **[1][9]** The resulting photoacoustic wave's amplitude is determined by the medium's thermodynamic constants (coefficient of compressibility: κ, thermal coefficient of volume expansion: β) and is proportional to the laser energy flux (F) and absorption coefficient (μ).

The photoacoustic effect was firstly discovered by Alexander Graham Bell in 1880**[10][11]**, when he was working on the development of photophone, a device that is useful for the transmission of speech on a beam of light. Because of the photophone , A. G. Bell and his partner Charles S. Tainter also discovered that illumination of different solid substances with a rapidly interrupted beam of light energy resulted in the emission of acoustic energy at the same frequency as the modulation frequency.

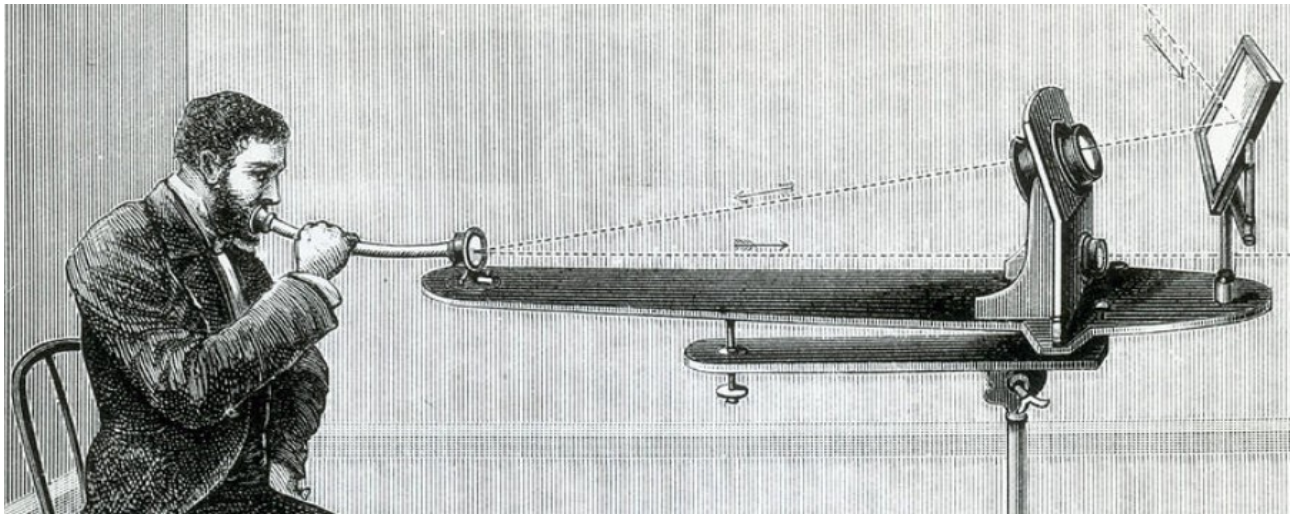

*Figure 4.2: Demostration of the Photophone **[12]***

After the discovery of the effect from Bell, for many decades there have been no further investigations or use of it. Although in 1938 the rival off the effect happened. Veingerov of the State Optical Institute, Leningrad, published a paper about a technology for infrared gas analysis using the photoacoustic effect.**[10][13]**

A year later, Pfund reported on a similar system in use at the Johns Hopkins Hospital for detection of CO and CO2 gases. With these works the theoretical foundation was developed for the optico-acoustic effect, and various implementations soon followed. In addition to gas concentration analysis, the method was also used in the investigation of vibrational relaxation rates and molecular energy transfer in gases. **[10][14]**

Then in 1960 with the development of laser the photoacoustic effect started to have other applications except of the gas analysis. To begin with in 1963 R.M. White developed the theory of thermoelastic wave generation in isotropic elastic bodies under several transient heating conditions **[10][15]**. In addition M.J. Brienza and A.J.

De Maria in 1967 **[10][16]** published a paper about Q-switched lasers, which produced strong ultrasonic waves due to the heating of metals of films surrounding the surface of piezoelectric crystals located at interior of lasers. Furthermore in 1977, R.J. O Von Gutfeld and R.L. Melcher **[10][17]** in a published paper, were the first to report the possible use of photoacoustic effect as an imaging technique. They set down the mechanical boundary conditions for thermoelastic expansion and reinforced at the same time the produced acoustic amplitude. To conclude Wickramasinghe et al. provided information about the development of a high-frequency acoustic microscope modified for photoacoustic studies. Light excitation was with short pulses (0.2 ns) from a mode-locked and Q-switched Nd:YAG laser at 1064 nm. Detection was performed using an acoustic lens and 800 MHz transducer. The first demonstration of an optical resolution photoacoustic microscopy was performed by Maslov et al in 2008. **[18]**

4.2.1 Acoustic Waves

An acoustic wave is defined as the propagation of a pressure disturbance within a material medium (solid, liquid, gas) through successive regions of condensation and rarefaction.

Most acoustic waves are longitudinal because the transmission direction matches the oscillation direction of the molecules. Some important quantities that characterize the acoustic wave are **[19][20][21][22]**:

i. Wave displacement amplitude (S_0): The maximum displacement from the equilibrium position
ii. Pressure wave width (P_0): The maximum pressure as a function of pressure value at equilibrium position.
iii. Speed of sound u_s: The rate of propagation in the medium
iv. Frequency f: the number of cyclic processes performed per second.
v. Intensity I: The emission or absorption rate of acoustic energy per unit of time.

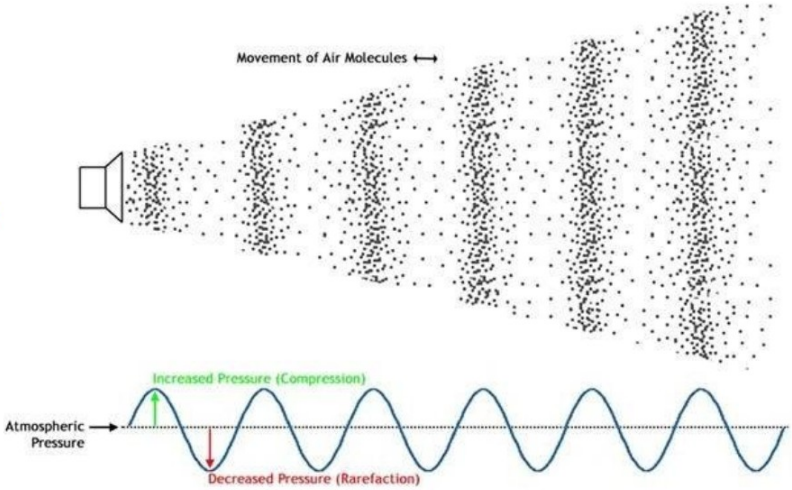

Figure 4.3: Propagation of sound with its impact pressure on air molecule in sinusoidal form

4.2.2 Reflection and transmission of acoustic waves

A sound wave, like any other wave, doesn't just stop when it hits a wall or another obstruction in its course. Instead, a sound wave will exhibit specific characteristics when it comes into contact with a barrier or the medium's limit. Diffraction around the obstacle, reflection off the obstacle, and transmission (together with refraction) into the obstacle or new medium are examples of possible behaviors. Great interest in photoacoustic effect has the transmission and the reflection of the waves. More specifically when an incoming acoustic wave reaches the boundary between one medium with acoustic impedance Z_1 another medium with acoustic impedance Z_2 a portion of the wave experiences reflection at the boundary and a portion of the wave is transmitted across the boundary when it reaches the boundary between two media. The degree of reflection depends on how differently the two media behave. This process is described mathematically by Snell's law $\frac{sin\theta_i}{sin\theta_r}=\frac{u_1}{u_2}$ (eq. 4.8), where θ_i is the angle of incidence , θ_r the angle of reflection and u_1, u_2 the velocities of sound in medium one and two.

Every medium that the acoustic wave is transmitted have a characteristic property ,the acoustic impedance Z which is the resistance to the propagation of

ultrasound waves through medium of dissemination. Acoustic impedance is the product of the density and speed of sound in the medium : $Z=\rho \cdot u_s[kg/m^2*sec]$ (eq. 4.9) . **[23]**

To conclude the transmission and reflection of acoustic waves is given quantitatively by the following equations:

Transmission Coefficient: $T=\frac{p_t}{p_i}=\frac{2Z_2 cos\theta_i}{Z_2 cos\theta_i+Z_1 cos\theta_t}$ (eq. 4.10)

Reflection Coefficient: $R=\frac{p_r}{p_i}=\frac{Z_2 cos\theta_i-Z_1 cos\theta_t}{Z_2 cos\theta_i+Z_1 cos\theta_t}$ (eq. 4.11)

In the case of vertical incidence we have θ_i= θ_t= 0 and the above equations take the form: $T=\frac{2Z_2}{Z_2+Z_1}$(eq. 4.12) and $R=\frac{Z_2-Z_1}{Z_2+Z_1}$ (eq. 4.13).

Also there is a general equation that connects the coefficients to each other for any angles : T= 1 + R (eq. 4.14).**[19][20][21][22]**. From the equations 4.12 and 4.13 someone could see that when Z_1=Z_2 the reflection coefficient becomes zero (R=0) and there is only transmission. This means that the whole acoustic wave is transmitted through a medium. On the contrary when Z_1<<Z_2 → $Z_2+Z_1\approx Z_2$ and $Z_2-Z_1\approx Z_2$, the reflection coefficient becomes maximum (R=1) and the transmission from the equation 4.14 is equal to two (T=2). In this case a significant part of the acoustic wave is reflected from the medium and the rest of it is transmitted. Also when Z_2<<Z_1 →$Z_2+Z_1\approx Z_1$ and $Z_2-Z_1\approx Z_1$, the reflection coefficient becomes minimum (R=-1) and the transmission from the equation 4.14 is quite small. Approximately someone could say that it becomes zero (T~0). This means that almost the whole acoustic wave is reflected from the medium.

4.2.3 The General Photoacoustic equation

The general photoacoustic equation that describes the production and transmission of photoacoustic waves is $(\nabla^2-\frac{1}{u_s}\frac{\partial^2}{\partial t^2})p(\vec{r},t)=\frac{-\beta}{\kappa u_s^2}\frac{\partial^2 T(\vec{r},t)}{\partial t^2}$ (eq. 4.15) where $p(\vec{r},t)$ denotes the acoustic pressure at location r and time t and T denotes the

temperature rise. The left side of this equation describes the wave propagation, whereas the right-hand side represents the source term.

To emphasize more into the general photoacoustic equation it is important to discover from where eg (eq. 4.15) generates. So the two basic equations responsible for photoacoustic generation are the thermal expansion equation and the inviscid force equation. The thermal expansion (generalized Hooke' law) is given by the equation $\nabla\cdot\vec{\xi}(\vec{r},t)=-\kappa\, p(\vec{r},t)+\beta T(\vec{r},t)$ (eq. 4.16) where the left-hand side represents the volume expansion, while the right-hand side represents the two factors related to the volume expansion :

- $\vec{\xi}$ denotes the medium displacement
- κ is the coefficient of isothermal compressibility:$\kappa=\frac{-1}{V}(\frac{\partial V}{\partial P})_T$
- β is the thermal coefficient of volume expansion : $\beta=\frac{1}{V}(\frac{\partial V}{\partial} T)_P$
- p characterizes the pressure
- T the temperature.

The linear inviscid force equation(the equation of motion) is $\rho\frac{\partial^2}{\partial t^2}\vec{\xi}(\vec{r},t)=-\nabla p(\vec{r},t)$ (eq. 4.17), where left-hand side represents the mass density times the acceleration, and the right-hand side represents the force applied per unit volume. Thus, Eq. 4.17 is an incarnation of Newton's second law. Taking the divergence of Eq. (4.17), we obtain $\rho\frac{\partial^2}{\partial t^2}[\nabla\vec{\xi}(\vec{r},t)]=-\nabla^2 p(\vec{r},t)$ (4.18). **[9][24]**

4.2.4 Photoacoustic Equation in thermal confinement

Generally speaking if the laser pulse width is much shorter than τ_{th} (thermal relaxation time, which characterizes the thermal diffusion), the excitation is said to be in thermal confinement, and heat conduction is negligible during the laser pulse. Likewise, if the laser pulse width is much shorter than τ_s (stress relaxation time, which characterizes the pressure propagation), the excitation is said to be in stress confinement, and stress propagation is negligible during the laser pulse. In order for

the following equations to hold, it is important in photoacoustics the laser to be in thermal and stress confinement, typically about 1ns.
By deriving the thermal equation $Q=mC_VT$ (eq. 4.19), where Q is the thermal energy, m the mass of the object, C_v the specific heat capacity under constant volume and T is the absolute temperature it is resulting to the equation below :

$$\frac{dQ}{dt}=mC_V\frac{dT}{dt}=\rho VC_V\frac{dT}{dt}\rightarrow[\rho C_V\frac{\partial T(\vec{r},t)}{\partial t}=H(\vec{r},t)(eq.4.20)]$$

, where $H(\vec{r},t)$ is the heating function defined as the thermal energy converted per unit volume and per unit time; it is related to the specific optical power deposition A_p by $H = \eta_{th}A_p$ and to the optical fluence rate Φ by $H = \eta_{th}\,\mu_\alpha\Phi$. Here η_{th} is the percentage that is converted into heat and μ_α is the optical absorption coefficient. Substituting Eq. (4.20) into Eq.4.15 , it can be obtained the following less general photoacoustic equation: $(\nabla^2-\frac{1}{u_s}\frac{\partial^2}{\partial t^2})p(\vec{r},t)=\frac{-\beta}{C_P}\frac{\partial H}{\partial t}$ (eq.4.21) .

The source term is related to the first time derivative of H. Therefore, time-invariant heating does not produce a pressure wave; only time-variant heating does. Sometimes, velocity potential φ_u—which is related to p as follows—is used : $p=\rho\frac{\partial\varphi_u}{\partial t}$ (eq. 4.22).

Substituting Eq. 4.22 into Eq. 4.21 yields the following equation, which avoids the time derivative of H: $(\nabla^2-\frac{1}{u_s}\frac{\partial^2}{\partial t^2})\varphi_u=\frac{\beta}{\rho C_P}H$ (eq. 4.23). **[9][24]**

4.3 Photoacoustic Microscopy (PAM)

Photoacoustic Microscopy is an imaging technique which by using the photoacoustic effect, can acoustically detect optical contrast and so illustrate better the image of the experimental sample. This happens because PAM overcomes the optical diffusion limit (~1mm) by taking advantage of the modest acoustic scattering in tissue while maintaining a high spatial resolution unlike conventional optical techniques. **[25][4]** Furthermore PAMs specificity depends on the fact that the variety of molecules in tissue absorb radiation at different wavelengths. As a

consequence based on the radiation's wavelength that has been used the acquired images diverge. For all these reasons PAM is widely used in biomedical for the imaging of the anatomical, functional, molecular, flow dynamic, and metabolic differences in tissues.

Photoacoustic microscopy can be divided into two kinds, optical resolution PAM (OR-PAM), where the visual focus is more dominant and acoustic resolution PAM (AR-PAM), where the auditory focus is sharper. The biggest difference of these two approaches of PAM is the fact that they have dissimilar range of oprical focus. Also in OR-PAM the laser beam is tightly focused but in AR-PAM it is diffused.

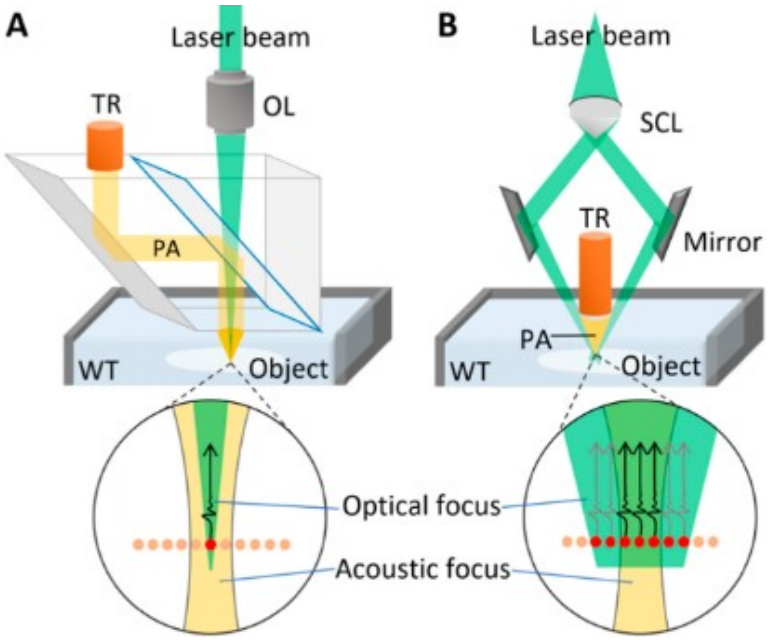

Figure 4.4 : Schematic illustration and representative images of OR- and AR-PAM systems. The typical configurations of (A) OR-PAM and (B) AR-PAM. The optical focus is smaller than the acoustic focus in OR-PAM, while the optical focus is larger than the acoustic focus in AR-PAM. The red and orange dots are excited and unexcited chromophores, respectively. The black and gray arrows are detected and undetected PA waves, respectively. ***[26]***

4.3.1 Optical Resolution PAM (OR-PAM)

OR-PAM offers high resolution (about 1 μm) but small focal depth (about 1 mm) which is mainly determined by scattering of light. Axial resolution is determined by the range of frequencies that the detector can distinguish while the lateral resolution from the focus of light. In OR-PAM there are used two kinds of microscopes. Firstly there are the microscopes on transmission mode, where the acoustic waves are transmitted in the same direction as the light and detected from a transducer, which is above the sample and aligned with the light source below it. Secondly there are the microscopes in reflection mode where the acoustic waves reflect on a surface and then they are detected from a transducer which is at a specific angle above the sample and aligned with the light source above it. In more detail in OR-PAM for both kinds of microscopes, a pulsed laser beam (~1 ns pulse) is focused on the sample with an optical lens. An optical-acoustic beam combiner is used for the coaxial and confocal alignment of optical illumination and acoustic detection. The resulting ultrasonic waves are first collected by a hollow acoustic surface at the bottom of the combiner and then detected by a broadband ultrasound transducer attached to the top surface of the prism. A correction lens is added to compensate for the optical aberration of the prism. The ultrasonic waves are recorded on a computer recording card where, using a special program, the following image is obtained and the sample is scanned point by point until the 3D image of the sample is formed.

The lateral resolution of the OR-PAM is given by the relation: $R_L = 0{,}51 \frac{\lambda_0}{NA_0}$ (eq. 4.24)with λ_0 the optical wavelength and NA_0 the numerical aperture of the objective. The constant 0.51 reflects the FWHM (full width at half maximum) of the optical focal point in light intensity. For the axial analysis, applies the relation $R_{axial} = 0{,}88 \frac{u_a}{\Delta f_a}$ (eq. 4.25) where Δf_a is the range of frequencies of the transducer and u_a the speed of sound. As we see from the equation 4.25, the axial resolution depends on the different time of arrival of the generated signals and is determined by the frequency range of the detector.**[25][27][28]**

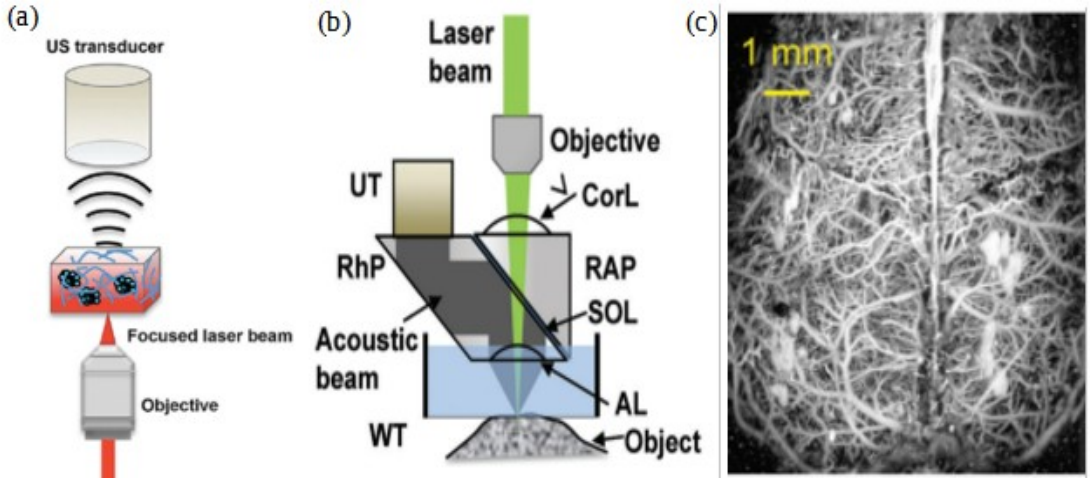

*Figure 4.5: Schematics of OR-PAM system: (a)1st Generation OR-PAM (b)2nd Generation OR-PAM (c)G2-OR-PAM of cortical vasculature in a living mouse with the scalp removed but the skull intact**[25][28]***

4.3.2 Acoustic Resolution PAM (AR-PAM)

This type of PA-microscopy presents a lower resolution but can be applied to a greater focal depth in a sample compared to OR-PAM. It is mainly applied in reflection mode, as it is designed for thick objects. The head of an acoustic analysis microscope consists of two mirrors and an acoustic piezoelectric detector (UT), elements on which its operation is based. In more detail, its operating principle is as follows: the laser beam passes through the head through a conical lens and provides a ring-shaped illumination area. Then, with the help of the two mirrors, the beam is weakly focused on the sample under study. In the center of the head is an acoustic piezoelectric detector, which is focused and records signals only from its focus and not from all areas of the sample. Now by moving this head over the sample photoacoustic waves are detected from the points where there is a light absorber, which then pass to the recording card and finally a 3D image of the sample appears.

Some characteristics of the AR-PAM are as follows. First, the loose focal region from the mirrors coincides with the focus of the detector. Also, the lateral resolution is related to how well the detector is focused, in essence to this in AR-PAM the optical beam is much wider than the acoustic focus, so the lateral resolution (25-30μm) is worse compare to the lateral resolution of OR-PAM. The lateral resolution is given by

the equation : $R_L = 0{,}71\frac{\lambda_A}{NA_A} = 0{,}71\frac{u_A}{NA_A f_A}$ (eq. 4.26), where NA is the numerical aperture of the ultrasonic transducer, u_A is the speed of sound in the medium, λ_A the central wavelength and f_A the central frequency of the signal. The constant 0.71 reflects the FWHM (full width at half maximum) of the acoustic focal spot in acoustic width. In contrast, its axial resolution is given by the same equation (eq. 4.25) as that of OR-PAM. In AR-PAM imaging depth is largely determined by ultrasound attenuation and much less by light scattering within the sample.**[25]**

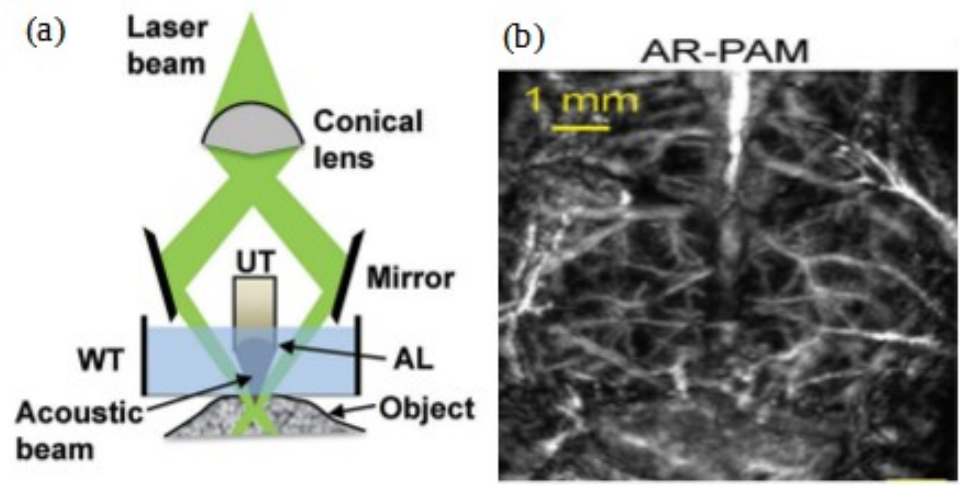

*Figure 4.6 :(a) Acoustic-resolution photoacoustic microscopy (AR-PAM) (b) Dark-field AR-PAM of the cortical vasculature in a living mouse with both the scalp and skullintact**[25]***

5.0 Optimization of Experimental Set-up

One of the main parts of this thesis was the construction and the optimization of an OR-PAM microscope. The main purpose of the optimization was to construct a system that offered clear acoustic signal with minimized noise while at the same time provide high resolution on all axes. With this purpose on mind, there was carefully selected a suitable combination of the optical and acoustic components in PAM and also for the selection of an appropriate lens, which would guide the ultrasound on the transducer. In addition it was taken under consideration which geometries of ultrasound transmission were more efficient to use in order to capture a high acoustic signal.

5.1 OR-PAM detection combinations

From the two kinds of PAM, this thesis focused on the construction and optimization of a reflection mode OR-PAM. In order to achieve efficient excitation and detection, separate paths are used. Despite that, it is difficult to build a suitable optical-acoustic combination for the best detection sensitivity. And so continuing, in reflection, the focused ultrasonic transducer cannot be placed directly underneath the lens without obstructing the optical focusing since the laser beam is sharply focused and the optical objective lens has a short working distance. In general transmission-mode and reflection-mode OR-PAM systems have been developed to achieve confocal alignment of the optical and acoustic beams. Nevertheless great interest is shown for the reflection mode OR-PAM, where the optical objective and ultrasonic transducer are all placed on top of the sample. In fact the sample thickness in not a limiting factor for reflection-mode OR-PAM. On the contrary the implementation of the system is more challenging, because it is hard to realize a large NA in both optical illumination, for high spatial resolution, and ultrasonic detection, for high sensitivity. **[29]**

There have been explored four methods for optical-acoustic combination in reflection-mode OR-PAM. To begin with the first method uses a customized ring-shape focused ultrasonic transducer, which has a central hole to pass the focused optical beam. Furthermore the ultrasonic transducer is coaxially aligned with the objective lens to a common focus. An alternative solution to this method is to use a specialized parabolic mirror with a conical hole to concentrate and reroute the ultrasonic waves. But unfortunately the acoustic focusing is impaired and there is at least 10% acoustic energy loss as a result of the central hole. The biggest disadvantage in this design is the lack of commercial availability of these ring-shaped transducers, which leaves very few options.**[29]**

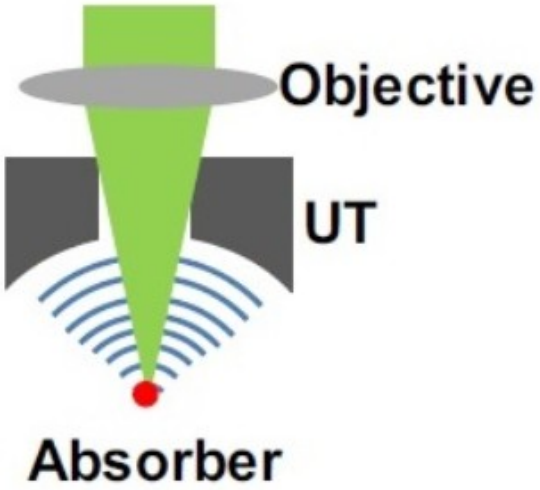

*Figure 5.1: A ring shape ultrasonic transducer (UT) is used with a central hole to pass the focusing laser beam**[29]***

The second method uses a customized optical-acoustic combiner to redirect the optical or acoustic beam. In this design, to achieve the confocal and coaxial alignment of the optical and acoustic beams, it is used a thin aluminum coating (100 nm thick)which is placed between two prisms and has the capacity to be optically clear but acoustically reflecting. The acoustic energy loss inside the combiner is negligible. However, this design is typically too big to be used with high NA objectives due to their short working distances. In addition the fact that only a flat transducer connected to an acoustic lens can be employed is another disadvantage. Also a 30% acoustic energy loss results from the acoustic impedance mismatch between the water (transmission medium) and the acoustic lens.**[29]**

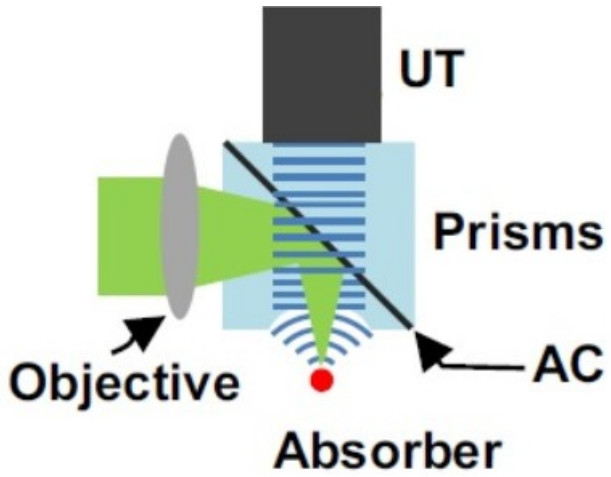

Figure 5.2 : An optical-acoustic combiner which is made of two prisms with a 100 nm thick aluminum coating (AC)layer in between ***[29]***

The third method uses a reflective dark-field optical objective. The objective and the ultrasonic transducer are aligned coaxially and confocally for maximum sensitivity More specifically the reflective dark-field objective has a long working distance (>20 mm) and as a result a commercial focused ultrasonic transducer can be placed directly underneath the objective. This design can achieve a large NA in both optical illumination (NA: 0.6) and ultrasonic detection (NA: 0.5). Moreover, an impedance matching layer can be coated to the ultrasonic transducer surface, and thus the acoustic energy loss due to reflection will be reduced. In addition, unlike a refractive based objective, the reflective objective can cover a wide wavelength range without degrading the optical-acoustic confocal alignment. It is a complex design, which its optimization is even more difficult.**[29]**This complexity is due to the fact that in this method a dark field microscopes should be used with a special condenser lens for the objective to illuminate the sample from the side or back, rather than from above, as in a traditional brightfield microscopes. Because the sample is illuminated from the side it is difficult for the beam to be focused on the sample. Furthermore the working distance of the objective is 20mm and as a result the sample should be placed 20 mm far from the objective, which is a distance quite far from the ultasound to traverse before detection.

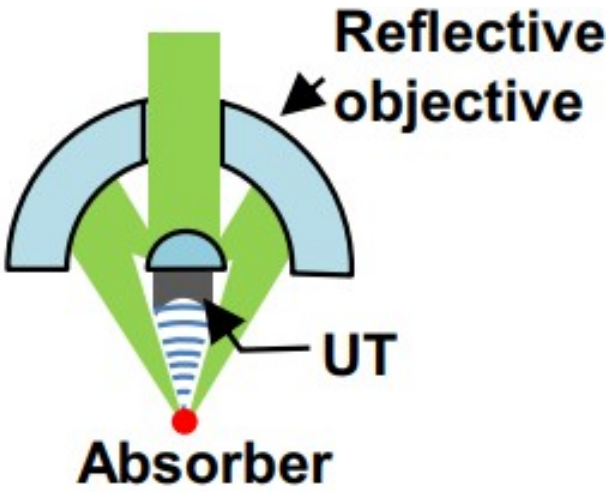

Figure 5.3: An optically reflective objective isused to form a dark-centered illumination pattern ***[29]***

Last but not least the fourth method uses a commercial ultrasonic transducer off-axis ,such as a needle transducer ,to the excitation laser beam. Signals generated in the overlap of the illumination and detection zones are detected, providing the additional benefit of quasi-dark-field detection. However, this design has a very limited acoustic NA (<0.2) and thus suffers from low detection sensitivity.**[29]**

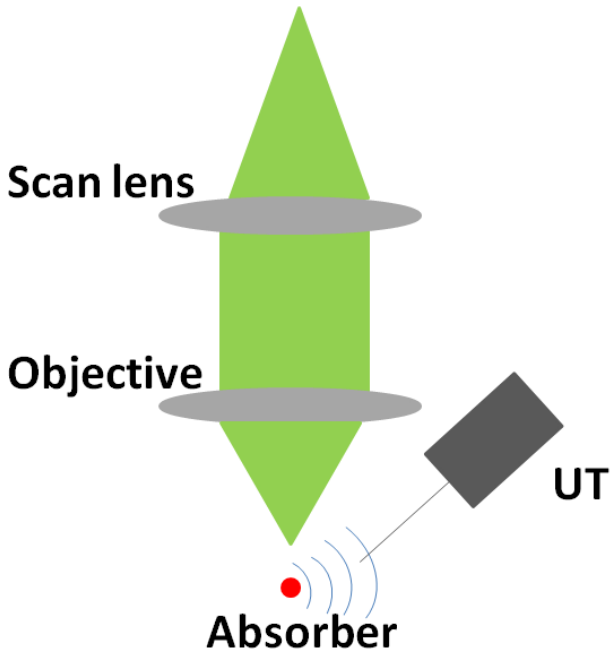

Figure 5.4: An off-axis transducer from the ecxitation laser beam

Taking into consideration the characteristics of each method, during this thesis it was used a variation of the second method which had as a customized optical-acoustic combiner a glass at 45° angle to redirect the acoustic beam. The advantage of this approximation is that unlike the beam splitter, did not present much sound attenuation. Furthermore this approach was preferred because compared to the first one it was easier to find commercial, the materials for its construction. On the other hand the third method was rejected due to the fact that it displayed a great complexity in the construction making especially difficult to be optimized. The fourth one had the biggest disadvantage of all because it depicts low detection sensitivity. The second method, that was selected, had the drawback that it displayed 30% acoustic energy loss. Nevertheless it was taken under consideration and by trying different lenses in front of the transducer for making the acoustic signal to focus better and different transmission modes it was improved and it will be analyzed later on.

5.2 Transmission modes of ultrasound

An important factor for the improvement of the acoustic signal is the transmission mode of the ultrasound that it was used. As it was mentioned previously it was decided that for the contraction and optimization of the reflection mode OR-PAM microscope would be use the second method for optical-acoustic combination. In accordance of this parameter there were studied two different approaches for the transmission of the ultrasound on the transducer, on a transmission mode microscope. Firstly it was measured the maximum value of the acoustic signal (V_{pp}) in transmission mode with the help of an already assembled experimental set up as shown in figure 5.5 **[30]**. Specifically the socket of the ultrasound detector and the acoustic was placed above the sample inside a water bath were the sample (black tape) was. There was nothing in between the sample and the transducer's socket. The objective(noMo, XB0098, NA: 0,1) was below the bath and the laser beam was focused on it from underneath. In the next measurement a beam splitter was placed inside the socket between the transducer and the lens. The beam splitter separates the optical from the acoustic beam (a mirror and a prism in contact:(a)Thorlabs MRA10-F01 10mm UV Enhanced Aluminum Right Angle Mirror (b) Thorlabs PS910 10mm Right Angle Prism). In comparison with the simple transmission before, this

time there was something in between the sample and the transducer's socket and as a result it was awaited that the ultrasound signal would be reduced. Then again an effort was made to measure the maximum value of the acoustic signal (V_{pp}) which proved the original prediction. Lastly the beam splitter was removed and a new transducer socket (Fig. 5.6) was used, which in the front had a glass at 45° angle. The incident acoustic beam on the glass, was reflected on an acoustic lens. This time also there there was something in between the sample and the transducer's socket but after the measurement of the maximum value of the acoustic signal (V_{pp}) ,the results were better. The process above was conducted five times with the power of laser in the simple transmission at I_0=1,77 mW and with the other two cases at I=4,3 mW ($I \sim 3 * I_0$).

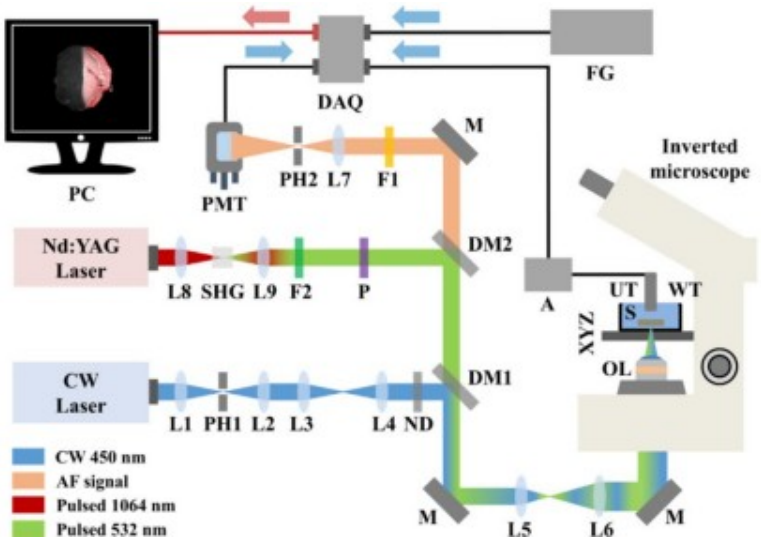

Figure 5.5 : Experimental Set up for OR-PAM in transmission mode with an Nd-YAG Laser ***[30]***

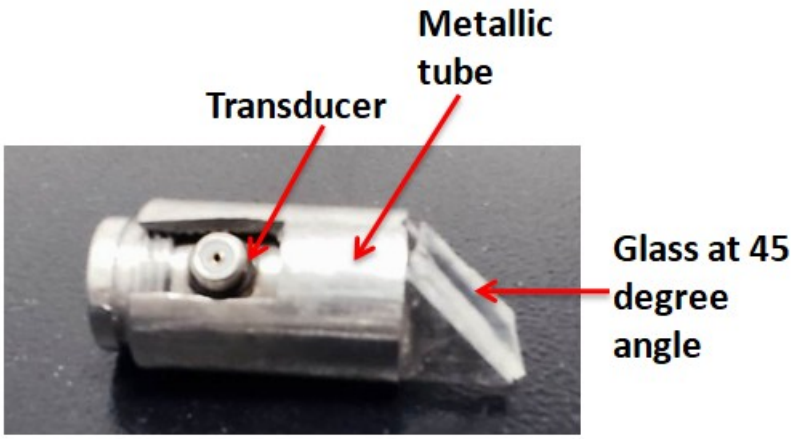

Figure 5.6: Socket of the transducer (metallic tube)

After the completion of the measurements, it was calculated the average value of V_{pp} of each approach and it was divided with lasers power that was used each time: $D(Direct\ Transmission)=\frac{V_{pp}^{tr}}{I_o}$ (eq. 5.1), $G(Glass)=\frac{V_{pp}^{gl}}{I}$ (eq. 5.2) and $B(Beamsplitter)=\frac{V_{pp}^{bs}}{I}$ (eq. 5.3). Finally the result of the division of the direct transmission mode, D, was used to normalize all results, in particular $\hat{D}=\frac{D}{D}=1$, $\hat{G}=\frac{G}{D}=0{,}61$ and $\hat{B}=\frac{B}{D}=0{,}03$. By combining then the values $\hat{D},\hat{G},\hat{B}$ and matching them with the appropriate transmission mode, the diagram 2 below emerged:

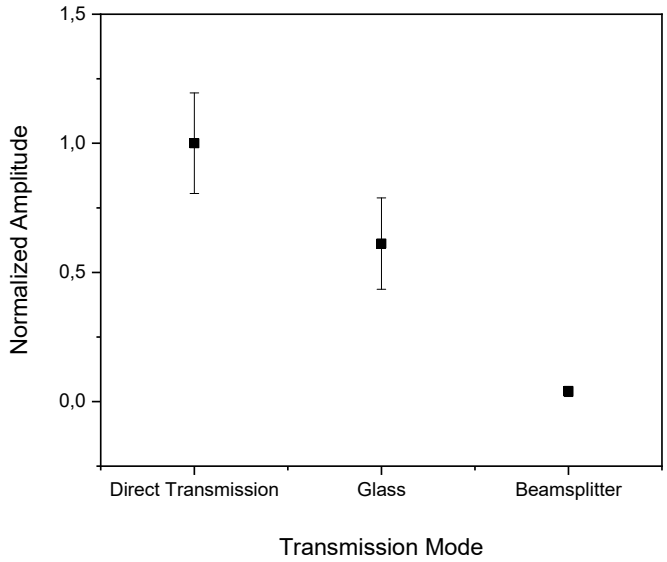

Diagram 1: The three transmission modes with their normalized signal amplitudes

From the diagram 2 someone can conclude that in an OR-PAM microscope in reflection mode, by using the socket with a glass at 45° the original acoustic was reduced and only the 61% of the original Vpp maximum value (direct transmission) was traceable as maximum. On the other hand by using a beam splitter almost all the acoustic signal was lost, because it could be detected only 0,3% of the original acoustic signal that the sample gave. Taking into consideration the above information, it was decided that it would be used a socket for the transducer and the

acoustic lens with a glass at 45° angle, because it would have produced better results on the sample's images and acoustic signal.

5.3 Acoustic lenses of the transducer

Like it was mentioned before it was studied and tested which acoustic lens in front of the transducer could give better results, specifically a bigger peak to peak acoustic signal amplitude (V_{pp}). The better signal is due to the fact that the lens guides the ultrasound on the active element of the transducer. First of all according to the theory above, the type of glass that the lens has been made of, affects the acoustic impedance (Z_1) because it depends of the density of material and the speed of sound inside the material. In addition the transducer itself has a glass, made from fused silica, on the surface with a specific acoustic impedance (Z_2) and as a result it is important the difference of Z_2 - Z_1 between the glass of the transducer and the acoustic lens to be as small as possible. Also the diameter of the lens should be bigger than the diameter of active element of the transducer for an efficient detection of the acoustic signal. This happens because if it is smaller, the fraction of the acoustic waves that reach the active element are less than the produced waves from the samples. Finally the acoustic focus (F_ac) of the lens should to be small enough to detect most of produced waves and record higher signal.

Taking into consideration all the above parameters it was estimate that there will be less losses of ultrasound signal and consequently better results, namely bigger V_{pp} , if a lens with small enough acoustic focus, with big diameter and from the same material as the glass of transducer was used. As a result, with the same system as above, there were studied 4 lenses made of different materials and with different acoustic focus and diameters to verify this reasoning. Specifically it was used the four commercially available lenses below in transmission mode to measure the respective maximum acoustic signal (V_{pp}) , under the same experimental parameters, laser beam power ~1,77-1,78 mW, wavelength ~532nm, excitation objective(noMo, XB0098) with NA=0,1 :

LENS	Model	Medium	Acoustic Impedance Z (kg/m^2 s)	Diameter D (mm)	Acoustic Focus F_ac (mm)
L1	LC-4291	Fused silica	13,19	8	7,3
L2	LC-2067	SF11	18,98	9	6,3
L3	LC-1975	BK7	15,18	6	16,4
L4	LC-2873	SF11	18,98	9	18,7

Firstly, a small quantity of ultrasound gel was used between the transducer and the lens to be in good contact and stable. Then the detector with the lens were placed inside a metallic tube which ensured a fixed alignment between them. Then the assembled tube was place in a water bath, were the sample (black tape) was in, and above it. The objective was below the bath and the laser beam was focused on it from underneath. By moving the stage of the sample, an attempt was made to find the maximum signal. The signal was displayed with an appropriate program software resembling an oscilloscope. This process was conducted ten times and in the end the average value of V_{pp} of each lens was calculated. The results are shown in the diagram 1 below:

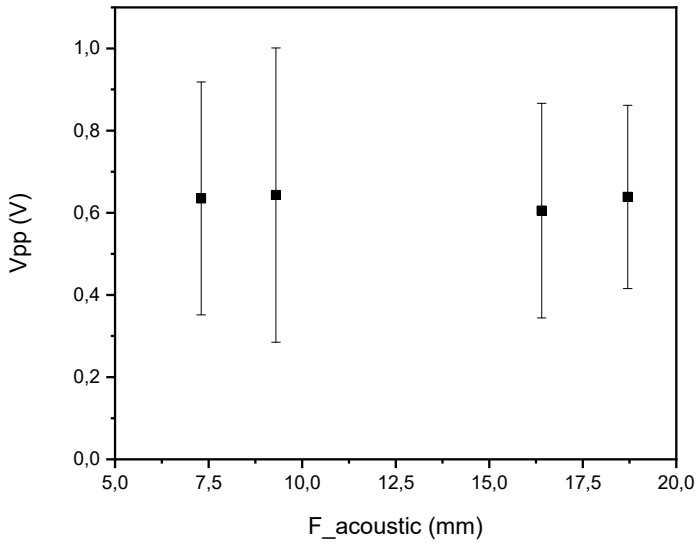

Diagram 2: The average Vpp of each lens and their respective acoustic focuses

As it appears above, the four lenses do not exhibit a significant difference between the average value of V_{pp}. Thus it is possible for someone to conclude that in the end it does not matter what lens has been used in front of the transducer. If there have been used four lenses from the same material, with equal diameters and different focal length, maybe the results would be variant. In addition the crucial factor for good signal was proved to be the alignment quality. Furthermore, there are two mechanical constrictions for the assembly of the transducer and the lens, the diameter of the transducer and the glass at 45° degrees. These constrictions create a minimum focal distance of approximately 12mm as shown in Figure 5.6.

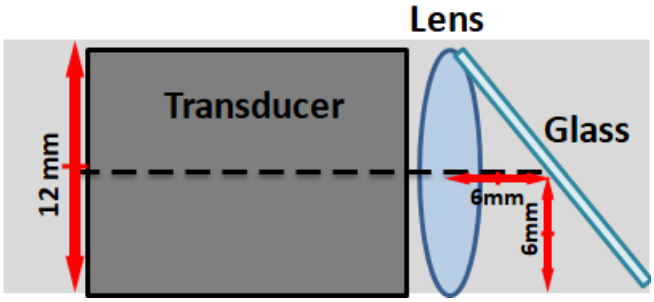

Figure 5.7 : Distances of acoustic and optical components in metalic tube

Taking into consideration the experimental results and the theoretical reasoning before and after the measurements there were two possible lenses that could be used the LC-1975 and LC-2873. Nevertheless it was preferred the diameter of the acoustic lens to be slightly larger than the diameter of the active element of the transducer (D>6mm), so that the sensor could receive acoustic frequencies in its entire range even with the slightest displacement of the lens on the transducer. To conclude it has been decided, the LC-2873 to be used because this lens had bigger diameter and as a result the transducer could detect on its whole width the produced acoustic frequencies

5.4 Experimental Set-up

After the selection of all the components, the experimental set-up that was constructed and used is shown in figure 5.8 and 5.9. It employed a reflection mode

configuration, with the light source above the sample and the ultrasonic detector oriented at 90° angle in between. As the light source was used a Coherent Helios laser which was emitting irradiation at 532nm with 1ns pulse width (repetition rate 10 kHz, power at 1,7 mW). For the ultrasound detection was used a transducer with frequency bandwidth at 83,44% having a central frequency of 70MHz.

An essential point to introduce is the direction that the laser beam follows. First of all, the initial beam from the laser enters a telescope, which consists of two lenses (L1 and L2, F1=75 mm, F2=150 mm) and thus the illumination beam becomes bigger. After the telescope there is a neutral density filter (ND), which has variable optical density and therefore reduces the power of the incident radiation to the desirable value. The the beam falls on a mirror (M1)(Thorlabs: BB1-E02 - Ø1" Broadband Dielectric Mirror, 400 - 750 nm) that reflects the beam in an upright microscope (the objective lens is above the sample) and it is driven to the objective (OL: MELLES GRIOT, Magnification 6,3, NA 0,17, Back focal length 160mm, Cover glass thickness 0,20mm). The objective focuses the beam on the sample and it is absorbed, and ultrasound is produced (photoacouatic effect). The produced ultrasound is transmitted with the help of water on the surface of a glass at 45° angle, where it is reflected towards an acoustic lens (L3: Thorlabs LC2873-A,SF11 A coated plano concave lens, Z=18,98, D=9, F_acoustic =18,7) in front of the transducer. The lens then guides the acoustic signal to the transducer where it is converted to an electrical voltage (V_{pp}). Then the acoustic signal is amplified inside an a low noise amplifier from few μV to hundreds of mV. This voltage is recorded on DAQ and then it is displayed on the computer screen with the help of a custom-made program software resembling an oscilloscope.
The sample is placed inside a water bath which is on top of a motor stage. This stage is moving so that the sample can be scanned (raster scanning) and as a result to take an image of it. For the sample to be depicted an appropriate program on computer is being used. Also the transducer and the acoustic lens (L3) are aligned together and placed inside a metallic tube, which has on the front a glass at 45° angle. This metallic tube is placed on top of a manual stage. The manual stage is used from the operator, to place the transducer (xyz axes) in the position that the detected acoustic signal is maximized maintaining at the same time the 90° angle in relation to the sample.

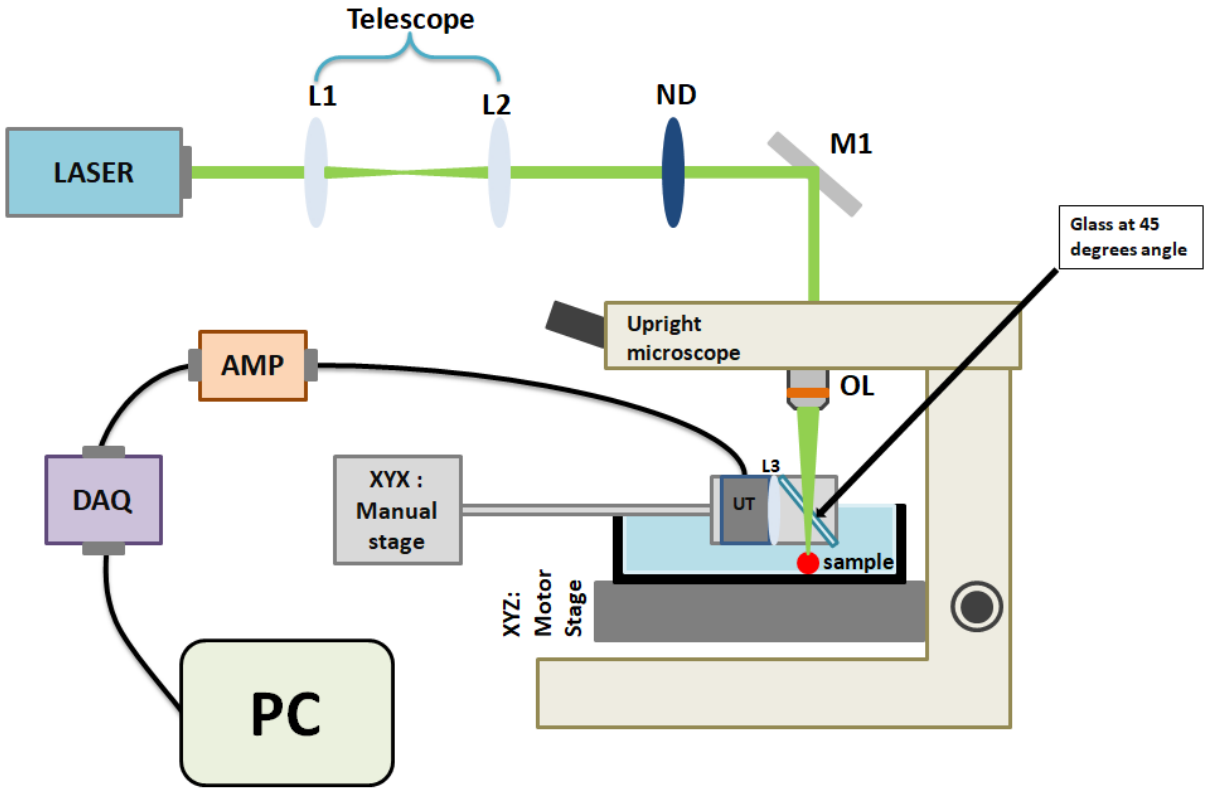

Figure 5.8: Schemetic demostration of the experimental set-up

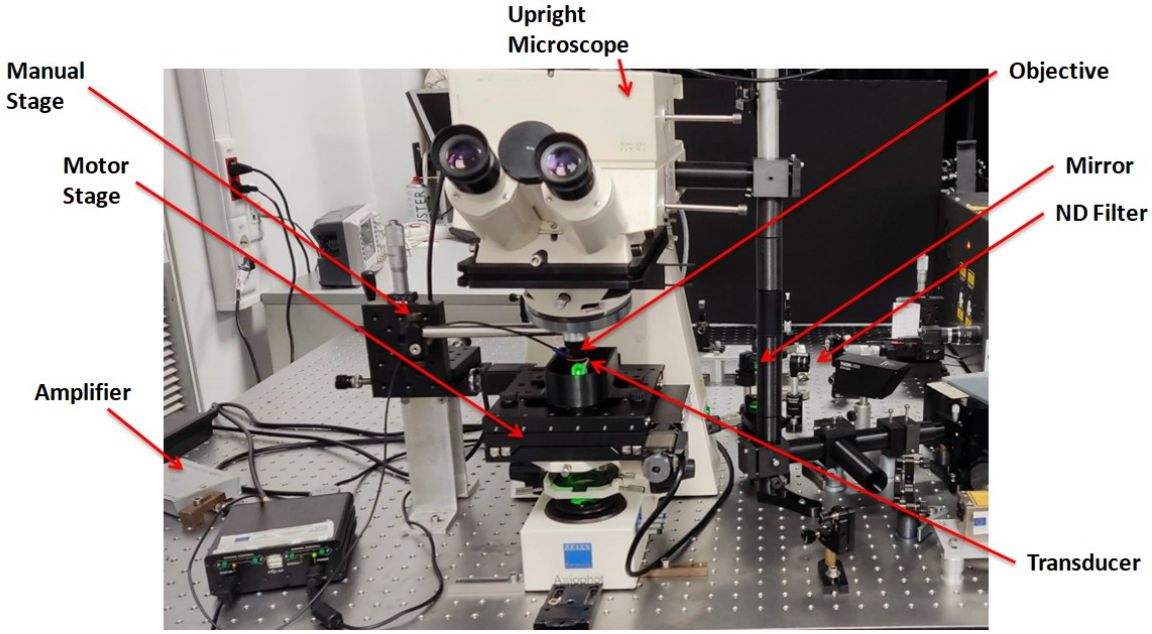

Figure 5.9 : The experimental Set- up

6.0 Characterization of the system

After the completion of the construction and the optimization of the experimental modality, attention was given to the characterization of the system. This included the measurement and determination of the signal to noise ratio (SNR), the frequencies that the transducer recorded and the field of view and depth of view.

6.1 General Experimental process

For the characterization of the imaging system different phantoms, which are specially designed objects that is scanned or imaged in the field of medical imaging to evaluate, analyze, and tune the performance of various imaging devices, were used as samples. To begin with, the phantoms were placed in a bath which had at the bottom a transparent glass. Then the bath was stationed on the motor stage of the set up and deionized water was added. Before the measurement of the acoustic signal the objective lens was used to focus the laser light on the phantoms. Next, the stage was moved so the laser was hitting the tape to acquire high ultrasound signal. The transducer and the objective with the help of the black tape were then aligned together. Then the aligned transducer and objective returned above the phantoms. Then the laser beam was guided from the top of the microscope to the objective which focused the beam on the sample where it was absorbed, and ultrasound waves were produced (photoacouatic effect). Then the produced ultrasound was transmitted on the surface of the transducer, where it is converted to an electrical voltage (V_{pp}). The acoustic signal was amplified inside an a low noise amplifier from few μV to several mV. This voltage was recorded on DAQ and then it was displayed on the computer screen with the help of a custom-made program software resembling an oscilloscope.

6.2 The Photoacoustic Signal and SNR

Following the experimental process it is time to present the produced acoustic signal that the set up could detect. The laser power after the objective lens was measured at 1,7mW and the averages values of each point, that the oscilloscope was counting,

were set to 10. Firstly, the shape of the acquired acoustic signal, which was shown at the oscilloscope was a diagram representing the amplitude of the photoacoustic pressure in Volts as a function of data points. Furthermore by knowing that the sampling rate of the DAQ was f=250MHZ, the sampling time for each point was determined according to the function $Time = \frac{i}{f}[ns]$, where i represent the point. Finally the diagram 3 below, which represented the photoacoustic signal in time, was formed:

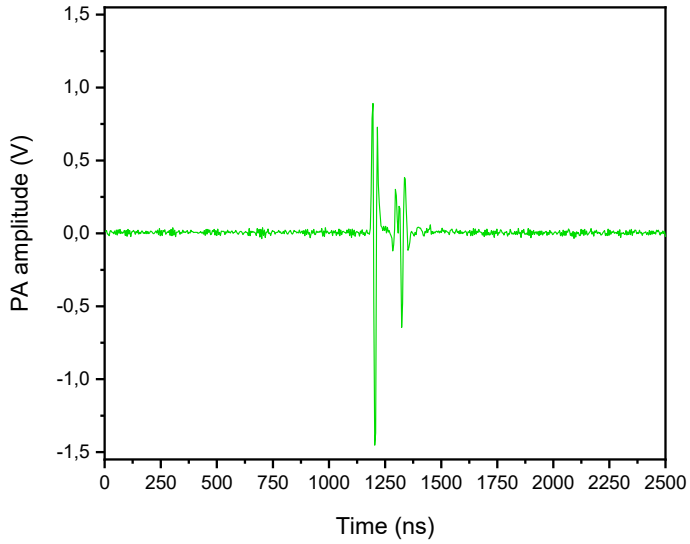

Diagram 3 : The produced PA signal as a function of time

According to diagram 3, the total recording time was depicted at 2500 ns ~2,5μs. In addition by observing the diagram from left to right, the following conclusions emerged. Initially, no signal appears until just before 1250ns, while at about 1250 ns the maximum amplitude of the signal appears, i.e. the thickening and thinning of the produced acoustic wave which had the values of 0.891 V and -1,453 V respectively. As a result the maximum amplitude was appraised at 2,344 V (peak to peak). Furthermore immediately after the PA signal, approximately between 1250-1500 ns, another signal appeared, which was due to reflection and scattering from the glass, on the bottom of the bath.

After the determination of the photoacoustic signal another important factor for the characterization of the system was the calculation of the signal to noise ratio (SNR) in order to compare the level of the desired signal with the level of background noise. To make this calculation possible, with the use of a suitable program, the standard deviation of the original data that the oscilloscope gave were estimated. It was found equal to stdev=0,01254 V. As it was mentioned above the maximum amplitude was V_{pp}= 2,344 V. By dividing these to quantities together the signal to noise ratio was calculated : $SNR = \frac{V_{pp}}{stdev} = \frac{2,344}{0,01254} = 186,9 \approx 187$. It became apparent that for only 10 averages the level of the detected photoacoustic signal of the system was really high compared to the background noise. Also the laser power we used is typical for biological samples. This hinted the existence of high contrast in future images of biological samples.

6.3 The recorded frequencies

Further on, the amplitude of the signal in the frequency domain was studied with the help of an appropriate program and using Fast Fourier Transformation on the initial waveform. The calculated frequencies was utilized to create a diagram of the amplitude of the photoacoustic as a function of the points. In the following diagram only the real (positive) frequencies are presented with normalized amplitude.

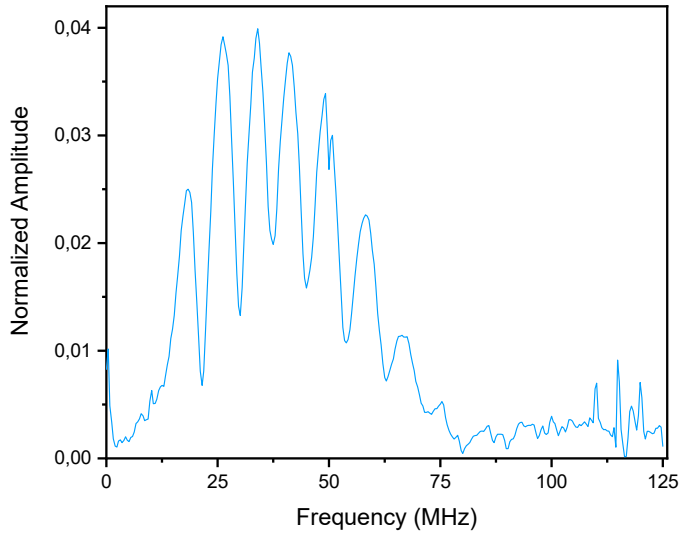

Diagram 4: The normalized PA signal amplitude as a frequency function

Firstly according to the Nyquist theorem the maximum frequency that the DAQ could detect would be equal to the half value of the systems sampling rate, namely the 250MHz. According to the diagram 4 the maximum frequency that was discovered was f=0,125 (1/ns)=125 MHz, value which was in harmony with the prediction that Nyquist theorem gave. It was mentioned in the description of the experimental set up that the ultrasonic detector exhibited sensitivity to frequencies between 40 and 100 MHz with central frequency at 70MHz**.** By comparing this information with the results of diagram 4, where the main contribution was shown around 25 to 70 MHz (main frequency range) approximately, they seemed in agreement. For frequencies higher than 100 MHz there was a contribution but it was quite smaller compared to the one inside the main frequencies range. At frequencies lower than 20 MHz small peaks were observed which may were due to noise. Also from the diagram 4 the maximum amplitude corresponded to frequencies lower than the expected value of 70 MHz, around 40 MHz. This happened probably because the sample (black tape) that was used for the measurement did not produce acoustic waves with such high frequency but mainly with lower such as 40MHz.

6.4 Depth of field and Field of view

As it was mentioned in theory the depth of field (DOF) is the range in which the object could still be clearly observed. Experimentally depth of field is considered the length over which the signal can be detected efficiently, which can be quantified with the full width at half maximum. The intensity of the signal was affected by three factors the excitation, the detection and how well their focuses convoluted. As a result the steps to determine the DOF experimentally were the following. To begin with, there has been used as a sample, a right angle prism with a black tape on the leaning side and a custom made software to take a picture. Later by processing the image in ImageJ and using the filters it provided, the contrast of the image was enhanced and the noise was effectively removed from the phantom area. In addition taking into consideration the pixel size of each dimension that the custom made software gave, the scale bar was set at 0,5 mm. The taken image is shown in figure 6.1(a) below:

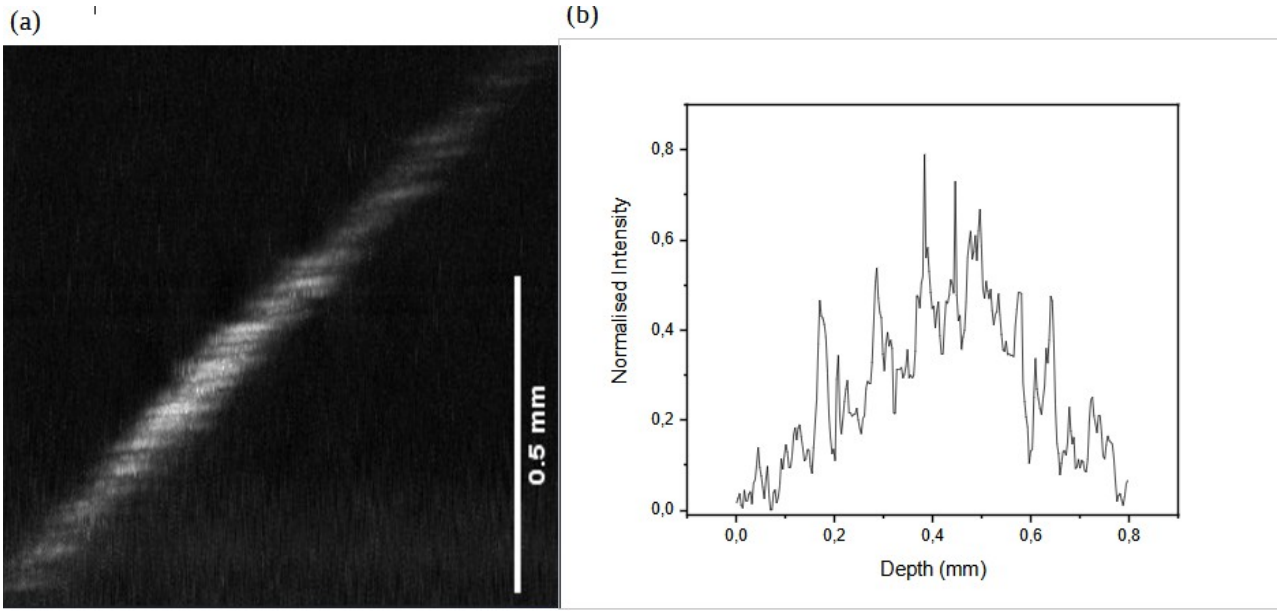

Figure 6.1: (a)Inclined Phantom (b) Profile of the bright area

In the low area of Figure 6.1(a), it was observed that there was strong absorption of light and therefore emission of ultrasound with a strong amplitude from the tape on the leaning side of the prism. As a result it appeared brighter compared to the surrounding area where the absorption is close to zero. Afterwards the data (gray values and diagonal distance) from the bright area was chosen to extract the intensity profile (Fig. 6.1(b)). In particular in the profile the depth was given by dividing the diagonal distance with $\sqrt{(2)}$ and also the initial intensity was normalized. The diagonal distance was divided with $\sqrt{(2)}$ because a right isosceles triangle was formed like the triangle in figure 6.2 below. Then by using the equation $sin\theta = \frac{opposite\ vertical\ distance}{diagonal\ distance}$, with θ=45°, which is equal to the angle of the used prism, the equation becomes $opposite\ vertical\ distance = \frac{diagonal\ distance}{\sqrt{2}}$, where the opposite vertical distance equals with the depth.

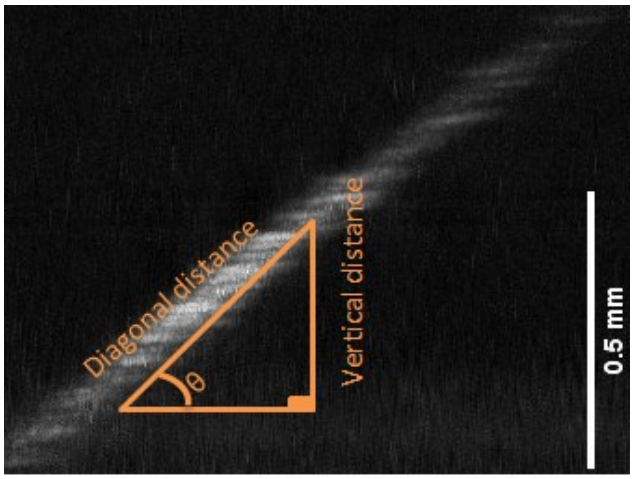

Figure 6.2: The right isosceles triangle

Finally according to the profile above, two methods were used to uncover the depth of view: i. applying a Gaussian fitting on the profile that would give the depth of field by calculating automatically the FWHM and ii. defining manually the maximum intensity and the FWHM on the profile after applying a 100 average fitting. It should be noted that the detector sensitivity does not exhibit a Gaussian form as the optical focus. The emerged diagrams are below:

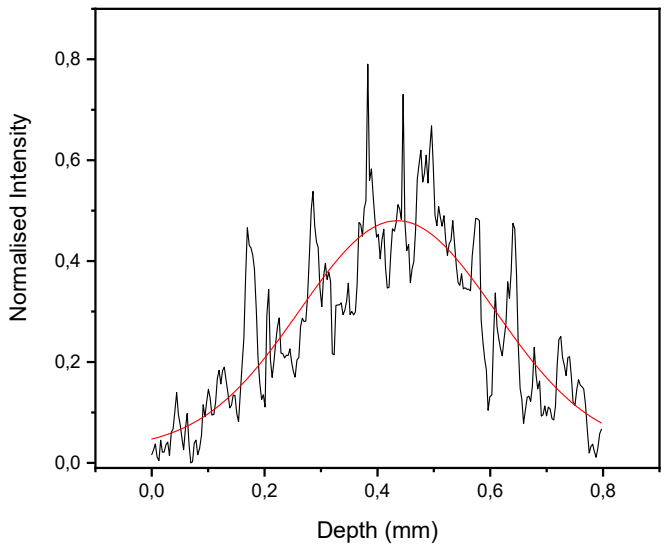

Diagram 5 : The profile with Gaussian Fit

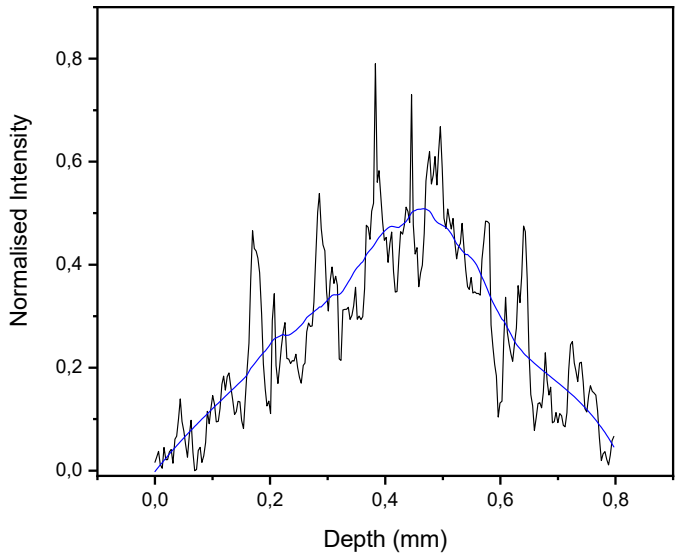

Diagram 6: The profile with the 100 average fit

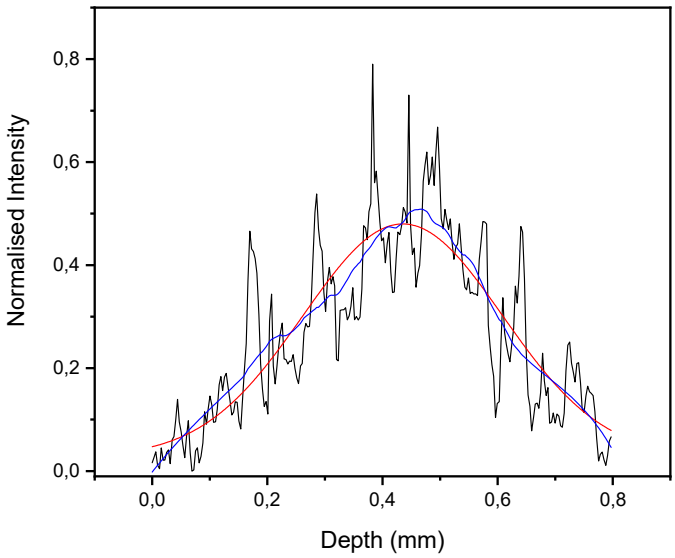

Diagram 7: The two fittings plotted together

In particular according to the diagram 7 the peak of the Gaussian was slightly left-shifted from the peak that the 100 average. This could be explained because of the fact that the detector sensitivity field does not exhibit a symmetric form as the optical focus. Also the depth of field with the first fitting method was found equal to

DOF_G=0,408mm. On the other hand with the second fitting the maximum intensity was approximately at 0,5 so the half is at 0,25 at x_1=0,204mm and x_2=0,624mm and so depth of field is equal to $DOF_A=x_2-x_1$=0,42mm. As shown by the results the two methods have given similar values to the DOF.

Regarding now the field of view (the extent of the observable area in distance units) of the system the restrictions are mechanical rather than optical. Specifically it is mostly mechanical limitations that depend on the free space between the walls of the bath and the metallic tube of the transducer. This space determines the range of movement of the motor stage and consequently the field of view. However it should be noted that by increasing the field of view the imaging time and the computational cost increase which also pose constraints when imaging biological samples.

In conclusion below is presented a first image that was received from the system (Fig. 6.3). The samples that were used, were carbon tubes with a diameter of 500 μm, which were placed one above the other and forming a cross.

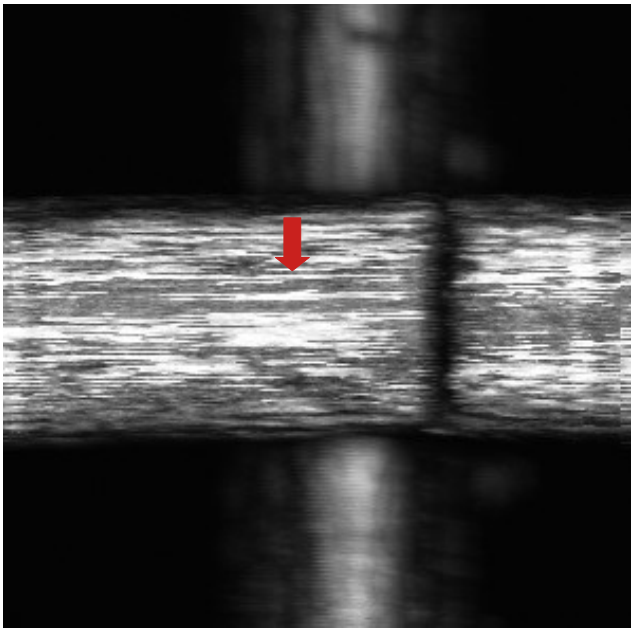

Figure 6.3: A standard image of two carbon tubes forming a cross (1,5mm x 1,5mm)

From the figure above, it seemed like the laser beam was tightly focused on the phantom above while the one below is blurry but clearly visible. In addition in the images appeared some motion artifacts (red arrow) that are due to the refraction of the laser beam from the moving water inside the bath. The stage movement speed

was 400μm/s which was lower than the usual speeds of such systems, which are around 2000μm/s.

7.0 Conclusion-Future works

During this thesis an OR-PAM microscopic system was successfully constructed. To begin with, each acoustic and optical component was optimally combined for the achievement of a reflection geometry mode OR-PAM microscope. This was achieved by using a metallic tube with a glass at a 45° angle and an appropriate acoustic lens to detect efficiently the ultrasound. Also during the characterization a high SNR was calculated. This gives the prospect of the existence of high contrast in future images of biological samples. Furthermore it was was found that the system could detect ultrasounds in a depth at least 0,4 mm. So in the future information about biological samples at maximum depth of 0,4 mm could be collected.

Nevertheless there are some further improvements that the system could have. Some of them are related to the artifacts that appear on the images. Firstly if there have been used a different and more stable to movement ultrasound medium than water, such as ultrasound wax, then during the movement of the stage there would have not been artifacts. Also instead of changing the medium another good idea is to use a different scanning method, which is based on the movement of the laser beam by using galvanometric mirrors (galvos). The usage of galvos can also increase the speed of scanning.

Others are related to the intensity distribution of the beam, namely instead of using a Gaussian laser beam a Bessel could be used, which retains its sharp focus for longer distance. With this in mind if molecules of a sample are one above the other, as in fig. 6.3, they could be both in tight focus from the objective. Finally, if the quality of the images is improved, it would be possible for the lateral and axial resolution of the OR-PAM system in reflection geometry to be determined. As a result a more complete OR-PAM system would be ready for biological imaging.

8.0 Acknowledgments

This current thesis was accomplished in Laboratory for Biophotonics and Molecular Imaging (LBMI) of the Institute of Electronic Structure and Laser (IESL) of FORTH. Since this work signifies the end of an important period, and it is a result of personal but mainly collective work, I would like to thank the people below. Firstly I would like to express my sincere gratitude to head of the laboratory Dr. Ioannis Zacharakis for accepting me and giving me the chance of fulfilling my thesis there and for always providing me with critical guidance throughout this period of time.
Furthermore I would like to thank the PhD candidate Mr. Konstantinos Mavrakis for his undivided support and additional perspectives in my research interest all these months. With his support and the long hours of discussions around the work and beyond, I learned more about bioimaging and fell in love with it.
In addition I would like express my gratitude to professor Charalambidis Dimitris (Physics Department Faculty Member) and Dr. Georgios Vassilakis (Principal Researcher), who accepted to be members of the evaluation committee of my thesis. Also I want to say thank you, to every new and old members of the LBMI for willing to answer my questions and for their encouragement when needed.
Finally, I would like to thank my family and friends for believing in me and supporting me during my studies and especially during this difficult period. Even the hardest days were brightened by them!

9.0 References

[1] Ntziachristos, V. (2010).*Going deeper than microscopy: the optical imaging frontier in biology.* Nature Methods, 7(8), 603–614. doi:10.1038/nmeth.1483
[2] The University of Edinburgh (2018). *What is Microscopy?*. Available at: https://www.ed.ac.uk/clinical-sciences/edinburgh-imaging/for-patients-study-participants/tell-me-more-about-my-scan/what-is-microscopy
[3] Ascoli, G. A., Bezhanskaya, J., & Tsytsarev, V. (2014). *Microscopy. Encyclopedia of the Neurological Sciences.16–20 d*oi:10.1016/b978-0-12-385157-4.00587-x
[4] Douglas B. Murphy, & Michael W. Davidson (2012). *Foundametals of light Microscopy and electronic Imaging*. 2nd edn. USA, Wiley-Blackwell. ISBN: 978-1-118-38290-5

[5] Marwan Abdellah, Thesis for Ph.D (2017). *In Silico Brain Imaging: Physically-plausible Methods for Visualizing Neocortical Microcircuitry.* doi:10.13140/RG.2.2.27464.21767

[6] Sotirios Bes, Kostantinos Kiritsis (eds) (2018) *Optics*. Eugene Hecht. 5th edn , Ahens, Gutenberg. ISBN:0133977226

[7] Wlliam Beaty (2004). *Lasers: What is Coherent Light?*. Available at :http://amasci.com/miscon/coherenc.html

[8] New York Microscope Company. Fred Koening (2019). *How to Estimate the Field of View of a Microscope.* Available at: https://microscopeinternational.com/how-to-estimate-field-of-view-of-microscope/

[9] Lihong V. Wang, Hsin-i Wu (2007). *Biomedical optics : principles and imaging;* ISBN: 978-0-471-74304-0

[10] Manohar, S., & Razansky, D. (2016).*Photoacoustics: a historical review. Advances in Optics and Photonics*, *8(4)*, *586*. doi:10.1364/aop.8.000586

[11] Bell, A. G. (1880).*On the production and reproduction of sound by light*. American Journal of Science, s3-20(118), 305–324. doi:10.2475/ajs.s3-20.118.305

[12] Bells Photophone Transmitter, 1880. Available at: https://fineartamerica.com/featured/bells-photophone-transmitter-1880-science-source.html

[13] Vengerov, M. (1946).*An Optical-Acoustic Method of Gas Analysis*. Nature, 158(4001), 28–29. doi: 10.1038/158028c

[14] Pfund, A. H. (1939). Atmospheric Contamination. Science, 90(2336), 326–327. doi: 10.1126/science.90.2336.326

[15] White, R. M. (1963).*Generation of Elastic Waves by Transient Surface Heating*. Journal of Applied Physics, 34(12), 3559–3567. doi: 10.1063/1.1729258

[16] Brienza, M. J., & DeMaria, A. J. (1967). *Laser-Induced Microwave Sound by Surface Heating*. Applied Physics Letters, 11(2), 44–46. doi:10.1063/1.1755021

[17] R. J. Von Gutfeld & R. L. Melcher, (1977). *MHz acoustic waves from pulsed thermoelastic expansions and their application to flaw detection.* Mater. Eval.35, 97–99.

[18] Maslov K., Zhang H., Hu S., (2008). Optical-resolution photoacoustic microscopy for in vivo imaging of single capillaries. Optics Letters, (33)9, 929. doi:10.1364/OL.33.000929

[19] R.W. Damon, W.T. Maloney, & D.H. McMahon (1970). 5-I*nteraction of Light with Ultrasound: Phenomena and Applications*. Physical Acoustics, Academic Press. 273-366. doi:10.1016/B978-0-12-395667-5.50011-8.
[20] Daniel T. Ginat, Vikram S. Dogra (2012). 19 - Future Considerations, Ophthalmic Ultrasonography. 201-207 , doi: 10.1016/B978-1-4377-2636-7.00019-7
[21] Simon R. Cherry, Ramsey D. Badawi, Jinyi Qi (eds)(2014). 4-Essentials of In Vivo Biomedical Imaging. U.S. ,CRC Press taylor & Francis Group. ISBN : 978-1-4398-9875-8
[22] The physics classroom (2022) . *Sound Waves and Music - Lesson 3 Behavior of Sound Waves*. Available at: https://www.physicsclassroom.com/class/sound/Lesson-3/Reflection,-Refraction,-and-Diffraction
[23] Mattoon, J. S., Nyland, T. G. (2015). *Fundamentals of Diagnostic Ultrasound*. Small Animal Diagnostic Ultrasound, 1–49. doi: 10.1016/b978-1-4160-4867-1.00001-5
[24] McDonald, F. A., & Wetsel, G. C. (1978). Generalized theory of the photoacoustic effect. Journal of Applied Physics, 49(4), 2313. doi: 10.1063/1.325116
[25] Yao, J., & Wang, L. V. (2013).*Photoacoustic microscopy*. Laser & Photonics Reviews, 7(5), 758–778. doi: 10.1002/lpor.201200060
[26] Jeong, W. Y., Kang, M. S., Lee, H., Lee, J. H., Kim, J., Han, D.-W., & Kim, K. S. (2021).*Recent Trends in Photoacoustic Imaging Techniques for 2D Nanomaterial-Based Phototherapy*. Biomedicines, 9(1), 80. doi:10.3390/biomedicines9010080
[27] Tserevelakis,G. J., Tsagaraki, M., & Zacharakis, G. (2016). *Hybrid photoacoustic and optical imaging of pigments in vegetative tissues*. Journal of Microscopy, 263(3), 300–306. doi:10.1111/jmi.12396
[28] Liu, W.-W., & Li, P.-C. (2020). *Photoacoustic imaging of cells in a three-dimensional microenvironment*. Journal of Biomedical Science, 27(1). doi: 10.1186/s12929-019-0594-x
[29] Yao, J., & Wang, L. V. (2014). *Sensitivity of photoacoustic microscopy*. Photoacoustics, 2(2), 87–101. doi: 10.1016/j.pacs.2014.04.002
[30]Tserevelakis G. J. , Pavlidis M., Samaras A.,. Barmparis G. D, Mavrakis K. G. , Draganidis I. , Oikonomou A. , Eleftheria Fanouraki2 , Tsironis G. P. & Zacharakis G. (2022). *Hybrid confocal fuorescence and photoacoustic microscopy for the label-free investigation of melanin accumulation in fish scales*. *Scientific Reports*. *Nature*. doi: 10.1038/s41598-022-11262-0